MR imaging of fetal head and neck anomalies

Caroline D. Robson, MB, ChB[a,b,*], Carol E. Barnewolt, MD[a,c]

[a]Department of Radiology, Children's Hospital Boston, 300 Longwood Avenue, Harvard Medical School, Boston, MA 02115, USA
[b]Magnetic Resonance Imaging, Advanced Fetal Care Center, Children's Hospital Boston, Harvard Medical School, 300 Longwood Avenue, Boston, MA 02115, USA
[c]Fetal Imaging, Advanced Fetal Care Center, Children's Hospital Boston, Harvard Medical School, 300 Longwood Avenue, Boston, MA 02115, USA

Fetal dysmorphism can occur as a result of various processes that include malformation (anomalous formation of tissue), deformation (unusual forces on normal tissue), disruption (breakdown of normal tissue), and dysplasia (abnormal organization of tissue).

An approach to fetal diagnosis and counseling of the parents incorporates a detailed assessment of family history, maternal health, and serum screening, results of amniotic fluid analysis for karyotype and other parameters, and thorough imaging of the fetus with sonography and sometimes fetal MR imaging.

Fetal imaging

Fetal sonography and MR imaging provide detailed sagittal, axial, and coronal views of the fetal facial profile. Sonography, however, can be limited by shadowing from ossified bone, particularly later in gestation. Because MR imaging does not have this limitation, sonography and MR imaging should be considered complementary modalities. MR images should not be interpreted in isolation or without full knowledge of the ultrasound greyscale and Doppler findings.

At the Children's Hospital, Boston, single-shot fast spin echo (SSFSE) T2-weighted images are primarily used for fetal MR imaging. When the fetal face is imaged, the sagittal view permits assessment of the frontal and nasal bones, hard palate, tongue, and mandible. Abnormalities include abnormal prominence of the frontal bone (frontal bossing) and lack of the usual frontal prominence. Abnormal nasal morphology includes variations in the size and shape of the nose. Macroglossia and micrognathia are also best diagnosed on sagittal images.

Coronal images are useful for evaluating the integrity of the fetal lips and palate and provide assessment of the eyes, nose, and ears. This view is also useful for the diagnosis of cleft lip (CL) or cleft palate (CP).

Axial images provide assessment of the neck and of the orbits and globes for measurements of interocular diameters for assessment of hypertelorism or hypotelorism. Normative values have been well established for sonography but not yet for MR imaging [1–3]. The maxilla, mandible lips, nasal cavity, and ears are also well seen. Ears may be abnormally small and low set or large and protuberant.

Abnormal masses such as cephaloceles, cystic vascular anomalies (eg, lymphatic malformation), and tumors (eg, hemangioma and teratoma) should be assessed using all three planes. Variations in morphology of the cranium resulting in brachycephaly, scaphocephaly, or turricephaly may indicate underlying craniosynostosis.

Concomitant anomalies involving the spine, heart, kidneys, or limbs and digits may provide additional clues to an underlying syndrome, sequence, or association. Several fetal craniofacial abnormalities are associated with an increased risk of aneuploidy.

---

* Corresponding author. Department of Radiology, Children's Hospital Boston, 300 Longwood Avenue Boston, MA 02115.

E-mail address: caroline.robson@childrens.harvard.edu (C.D. Robson).

(Aneuploidy is the term used to denote an abnormal number of one or more chromosomes or to signify that a piece of chromosomal material is lacking or in excess.)

First-trimester sonography may fail to detect craniofacial disorders that may become progressively apparent over time. Should a craniofacial anomaly be detected, fetal chromosomal analysis is often indicated. Antenatal detection of anomalies during the late second or third trimester may provide information that is useful in determining delivery strategy and in planning of subsequent perinatal and neonatal treatment including surgical intervention and methods to secure the fetal airway during delivery or in the perinatal period.

Cleft lip/cleft palate

CL/CP is the most common anomaly of the fetal face and occurs in approximately 1.2 to 1.3 of 1000 live or stillbirths [4,5]. CL/CP is more common in males and has been linked to genetic and environmental causes.

The antenatal detection of CL/CP necessitates parental counseling about possible associated anatomic abnormalities and aneuploidy, as well as the clinical and surgical implications of the cleft. The clinical manifestations include cosmetic deformity and functional impairment. The Online Mendelian Inheritance in Man (OMIM) and the National Center for Biotechnology Information database at the National Library of Medicine lists 198 genetic conditions associated with CL/CP [6]. The most commonly associated chromosomal abnormalities include trisomies 18 (unilateral CL/CP) and 13 (bilateral CL/CP) [5]. The prevalence of other malformations associated with CL/CP is approximately one in three infants following live birth [7]. The incidence of associated trisomies and multiple, potentially lethal malformations is much higher (up to 80%) in conceptuses with CL/CP than in live-born infants [8,9]. In an extensive population-based study in Utah, Walker et al [5] found that when additional major anatomic abnormalities are present by sonography, the risk of aneuploidy is approximately 17% for isolated CL, 22% for unilateral CL/CP, and 43% for bilateral CL/CP. The most common major anatomic abnormalities are cardiac, skeletal, or facial (hypertelorism) or affect the central nervous system [5,7]. Central nervous system anomalies include microcephaly, microphthalmia, and anopthalmia [5]. When no major anatomic abnormalities are detected by sonography, the authors found that the risk of an additional major abnormality at birth is

approximately 7% for unilateral CL, 17% for unilateral CL/CP, 8% for bilateral CL, and 21% for bilateral CL/CP [5]. Midline CL/CP is a distinct entity that forms part of the holoprosencephaly spectrum and trisomy 13 [9].

During normal development the upper lip and palate form between the fourth and ninth weeks of gestation [5]. Normal formation of the upper lip and palate requires fusion of the paired medial nasal processes and paired maxillary processes. Failure of fusion results in CL or CP. The primary palate is the portion of the hard palate located anterior to the incisive foramen. The secondary palate lies posterior to the incisive foramen.

Isolated CL occurs in approximately one third of cases. CL/CP occurs in approximately two thirds of cases [10]. Clefting of the alveolus almost always coexists with CL; however isolated CP is not usually associated with an alveolar cleft and is difficult to detect antenatally [4]. Anomalies associated with CL/CP include abnormalities of dentition, incomplete growth of the ipsilateral alar nasi, and mild hypertelorism.

The distinction between the different types of CL/CP is important in terms of the timing of postnatal surgery, need for presurgical orthopedic or dental manipulation, and design of the surgical repair. Fetal imaging provides useful information about CL/CP that may assist in antenatal counseling. In evaluating CL/CP, one should try to document whether the cleft is complete or incomplete and unilateral or bilateral, to detect the extent of alveolar clefting, and, if possible, to determine whether there is extension of the cleft into the secondary palate. CL/CP that extends to the secondary palate tends to affect speech, swallowing, and sucking and is associated with chronic middle ear infections. If the CL/CP is bilateral, the clefts can be symmetric or asymmetric, and the degree of premaxillary proclination should be noted [11].

A unilateral cleft involves one side of the lip (Fig. 1). When tiny or minor, a cleft is sometimes termed a microform and can be cryptic on imaging. Bilateral clefts involve both sides of the lip (Fig. 2). An incomplete cleft does not extend through the nasal floor. A complete cleft lacks tissue connection between the nasal floor and premaxilla (Figs. 1,2). Sometimes, however, a band of tissue connects the medial and lateral side of a complete CL. Bilateral complete clefts are usually associated with protrusion of the intermaxillary segment, which can be detected by ultrasound [12] and MR imaging (Fig. 2). Both the degree of protrusion and asymmetry affect surgical management [11]. Prenatal sonography is an impor-

Fig. 1. Unilateral right complete cleft lip and palate (CL/CP) imaged at a gestational age of 27.5 weeks. (*A*) Fetal sonography in the coronal plane reveals a unilateral right complete CL/CP (*arrow*). (*B*) Sagittal SSFSE T2-weighted MR image reveals the high signal intensity amniotic fluid extending from the oral cavity (*short arrow*) to the nasal cavity (*long arrow*), delineating the complete CP. (*C*) Coronal SSFSE T2-weighted MR image reveals the wide complete CP (*arrow*) with amniotic fluid extending from the oral cavity into the right nasal cavity. Compare with the left side, where the hypointense nasal septum extends inferiorly to meet the hypointense left side of the hard palate. (*D*) Axial SSFSE T2-weighted MR image demonstrates the CL/CP with interruption of the alveolar margin (*arrow*).

tant modality for characterizing the type and extent of CL/CP, because the extent of the cleft correlates with fetal outcome and associated anatomic and karyo-typic abnormality [9,13].

The rate of antenatal sonographic detection of CL with or without CP ranges from 22% to 73% of cases [14]. Diagnostic accuracy depends on obtaining correct anatomic views in the presence of adequate

amniotic fluid. Depiction also depends on separation of the margins of the cleft. The detection rate for CL improves with advancing gestational age, especially when the scan is obtained at or after 20 weeks' gestation [14]. In expert hands, ultrasound has been found to be accurate in differentiating unilateral from bilateral clefts and in distinguishing isolated CL from CL/CP [13,15,16]. The extent of involvement of the
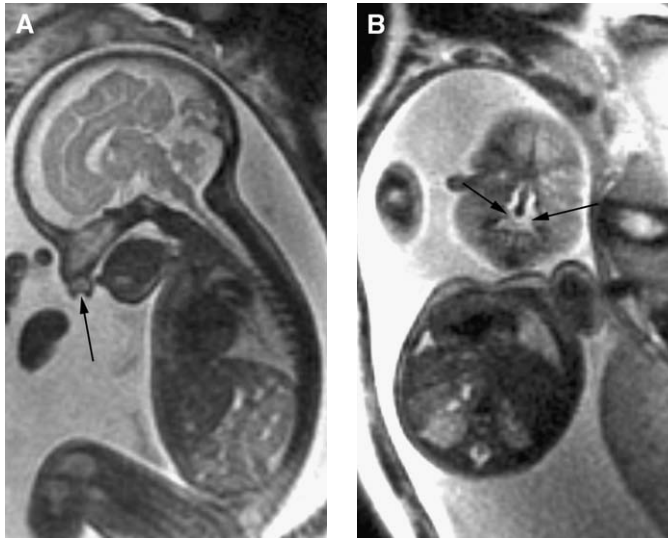
Fig. 2. Bilateral complete CL/CP imaged at a gestational age of 32 weeks, 4 days. (*A*) Sagittal midline MR image of the fetus reveals the protruding premaxillary segment (*arrow*) that is associated with bilateral complete CL/CP. (*B*) The coronal image reveals the bilateral complete CL/CP (*arrows*). Note the midline hypointense nasal septum separated from the tongue by hyperintense amniotic fluid.

alveolus and detection of a cleft extending to the soft palate may be difficult, however, because of acoustic shadowing from the facial bones. Sonographic visualization of the soft palate is unreliable, but clefting may be suggested by motion of the tongue above the level of the hard palate or by the reflux of amniotic fluid into the nasal cavity on color Doppler ultrasonography [17]. Although a cleft of the hard and soft palate is often assumed to be present if there is a wide CL, in about 10% of these infants the secondary palate is in fact intact [11]. Nyberg et al [13] proposed a prenatal ultrasonographic classification of CL with or without CP. CL alone was classified as type 1; unilateral CL and CP as type 2; bilateral CL and CP as type 3; midline CL and CP as type 4; and facial defects associated with amniotic bands or limb-body-wall complex as type 5. Berge et al [9] proposed adding isolated CP to the Nyberg classification.

Fetal MR imaging of CL/CP has recently been described [10,18]. Axial, coronal, and sagittal images diagnose the side of unilateral clefts, demonstrate involvement of the alveolar margin and anterior palate, and differentiate between unilateral and bilateral clefts (see Fig. 1). Coronal images are particularly useful for demonstrating distortion of the nose, which can be a useful indirect indicator of a defect involving the alveolus [10]. As with sonography, anterior protrusion of the premaxilla on sagittal images is a useful indicator of bilateral clefting (Fig. 2A). MR imaging is sometimes limited if

amniotic fluid does not fill the nasal and oral cavity. The normal palate, however, can often be seen as a hypointense line separating the fluid within the nasal cavity from the fluid within the oral cavity on SSFSE T2-weighted images. Provided there is adequate fluid within these spaces, CP is suggested if the hypointense palate is not seen [10]. The accuracy of this technique in a large series of patients with CL/CP has not, as yet, been published.

Facial clefts

A cleft is defined as an interruption of either soft tissue or bone [19]. Craniofacial clefts other than CL/CP are rare. Craniofacial clefts can occur around the orbit and eyelids, around the jaws and lips, or in both locations. The Tessier [19] classification for facial, craniofacial and laterofacial clefts gives a numeric assignment to the axes of various types of clefts. Tessier based his classification on the physical examination of 336 affected patients and surgical findings in 254 of these. He observed that bones and soft tissues are rarely involved to the same degree. From the midline to the infraorbital foramen, defects of soft tissue are more frequent or more severe; from the infraorbital foramen to the temporal bone, bony defects are more severe, with the exception of malformations of the pinna. Microphthalmia or epibulbar cysts are associated with orbital clefts.
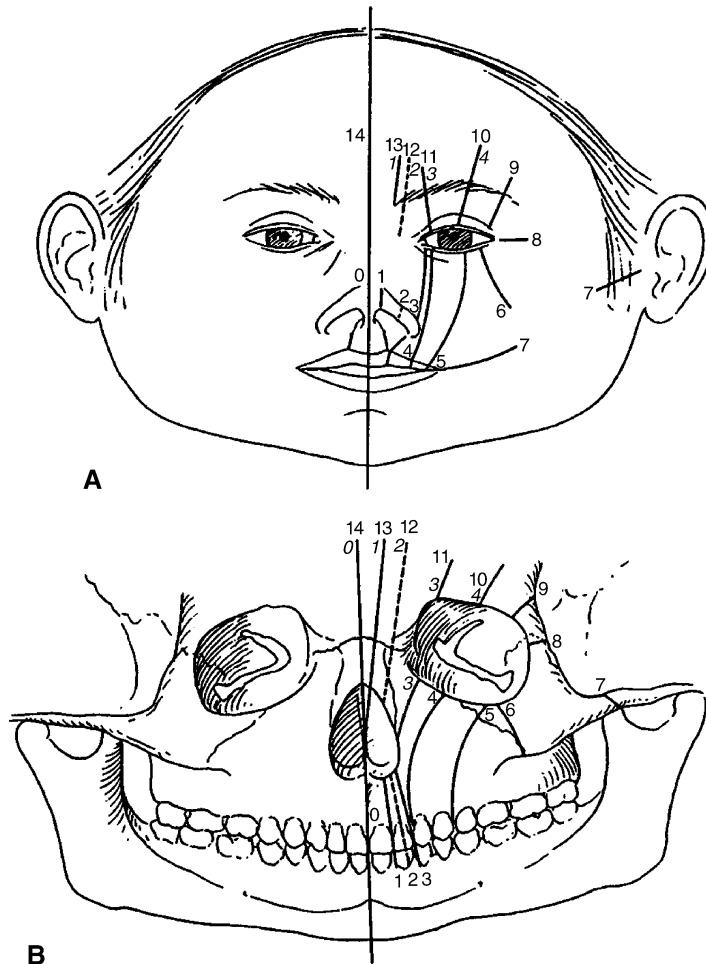
Fig. 3. Tessier craniofacial clefting system. (*A*) Soft-tissue clefts. (*B*) Bony clefts. Dotted lines represent uncertain localization or uncertain clefting. (*From* Cohen Jr MM. Asymmetry: molecular, biologic, embryopathic, and clinical perspectives. Am J Med Genet 2001;101:292–314; with permission.)

An adapted diagrammatic depiction of Tessier's facial and cranial clefts demonstrates the 15 locations for clefts, with 0 assigned to median facial dysraphism (Fig. 3) [19,20]. Facial clefts are numbered 0 through 6; cranial clefts are numbered 9 through 14. Cleft 7 occurs laterally toward the ear, and cleft 8 extends laterally from the orbit. Clefts 8 through 14 extend around the lateral or superior aspect of the eye.

Cleft 0 or 14 is associated with median facial cleft syndrome, frontonasal dysplasia and holoprosencephaly, absence of the premaxilla, and arrhinencephaly. Median facial anomalies manifest as tissue deficiency or disorders with normal or excessive amounts of tissue with cephaloceles (Fig. 4). Median anomalies with a deficiency of

tissue produce median cerebrofacial dysgenesis with resultant characteristic facial and orbital malformation and holoprosencephaly [21]. At the severe end of the spectrum is alobar holoprosencephaly. The most severe ocular and nasal findings associated with alobar holoprosencephaly are a single or partially divided eye in a single orbit (cyclopia) or anophthalmia, with absence of the nose (arrhinia) or a double proboscis. Ethmocephaly refers to extreme hypotelorism with arrhinia or a double proboscis. Cebocephaly refers to orbital hypotelorism with a proboscis-like nose. The mildest associated finding is median CL (premaxillary agenesis) with orbital hypotelorism, a flat nose, and absence of the upper lip [21]. Semilobar or lobar holoprosencephaly are associated with orbital hypotelorism, bilateral CL,
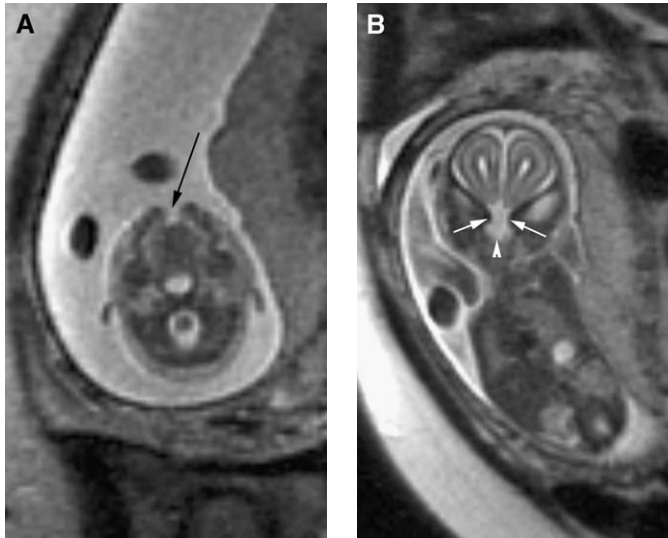
Fig. 4. Median cleft lip in a fetus imaged with MR at 21.5 gestational weeks. (*A*) Axial SSFSE T2-weighted image reveals a median cleft lip and palate (*arrow*). (*B*) Coronal image demonstrates a defect in the sphenoid bone within the central skull base (*long arrows*). A fluid-filled sphenoidal cephalocele (*arrowhead*) protrudes through the defect into the nasopharynx. There was also agenesis of the corpus callosum (not shown).

and nasal flattening with a flattened nose, pyriform aperture stenosis, and a single central mega incisor.

Cleft lip is most frequently encountered with Tessier clefts 1, 2, or 3. Hemiatrophy of the nose, supernumerary nostrils (Fig. 5), and proboscis lateralis are probably different manifestations of the same defect [19]. Tessier clefts 6, 7, and 8 are found in syndromes with malar and mandibular hypoplasia with variable bony defects of the maxilla, mandible, and zygoma. Some of these clefts occur in lateral
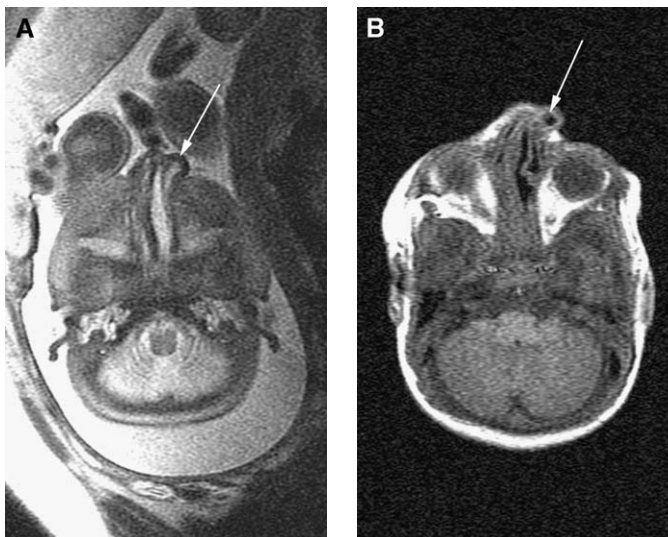

Fig. 5. Fetal MR image obtained at 32 weeks' gestation to evaluate further suspected fetal cephalocele detected on antenatal sonography. (*A*) Axial SSFSE T2-weighted image reveals an elongated fluid-filled structure (*arrow*) adjacent to the fluid filled left nasal cavity. A differential diagnosis of cephalocele or cystic neuroglial heterotopia was given. Following delivery a clinical diagnosis of a supernumerary nostril was made and confirmed with MR imaging. (*B*) Axial SE T1-weighted MR image reveals the supernumerary nostril that now contains air (*arrow*).

facial microsomia (hemifacial microsomia, Goldenhar's syndrome, Franceschetti complex) and Treacher Collins syndrome [19,21].

Amniotic band sequence

The amniotic band sequence consists of soft tissue derangements that have been postulated to arise from tethering of the fetus by fibrous bands of amniotic tissue, amniotic rupture, abnormal blastogenesis, vascular disruption, or genetic mutation with a human homologue of the disorganization phenotype [22–24]. Amniotic band sequence manifests as craniofacial, thoracic, abdominal, or limb involvement with limb reductions, ring constrictions, and skin amniotic adhesions. Craniofacial involvement includes features such as acrania, cephalocele, typical or atypical facial clefts, and eyelid coloboma [23]. Anencephaly has been diagnosed on fetal MR imaging, resulting in termination of pregnancy, with a subsequent diagnosis of amniotic band sequence made on fetal autopsy [25].

Micrognathia and retrognathia

Micrognathia refers to an abnormally small mandible (abnormal size). This condition must be differentiated from retrognathia, which is a receding chin (abnormal position) [26]. These two findings often co-exist. Micrognathia and retrognathia can be sporadic or inherited, and isolated or part of a syndrome. OMIM lists more than 200 genetic conditions associated with micrognathia and at least 30 associated with retrognathia [6]. Chromosomal abnormalities have been reported in 25% to 66% of fetuses with micrognathia [27,28]. These abnormalities include trisomies, 13, 18, and 9 [28]. For this reason, the antenatal detection of micrognathia or retrognathia mandates detailed assessment of the fetus for additional anomalies, genetic consultation, and special preparation for delivery with immediate airway support.

Most fetuses with micrognathia have additional anatomic anomalies, and these other findings tend to be predictive of a poor outcome. Micrognathia and retrognathia can be associated with narrowing and sometimes complete obstruction of the airway. Mandibular hypoplasia also tends to displace the tongue superiorly, which, in turn, prevents normal development of the palate, resulting in a palatal cleft, as discussed later in the Robin sequence [29]. Antenatal polyhydramnios and postnatal feeding difficulties can also occur. Even with the antenatal detection of apparently isolated micrognathia, there is a high probability of isolated CP without CL (rarely identified on antenatal sonography), possible respiratory difficulty at delivery, or developmental delay [30].

Fig. 6. Severe micrognathia in a fetus imaged at 32 weeks', 6 days' gestation. (*A*) Sagittal SSFSE T2-weighted MR image demonstrates severe micrognathia. (*B*) Ultrasound image of the hand reveals abnormally approximated position of the third to fifth fingers Postnatally, a diagnosis of Nager's syndrome was made.

Antenatal diagnosis of micrognathia or retrognathia can affect the timing and mode of delivery as well as management of the airway.

With sonography or MR imaging, sagittal images are best for the detection of micrognathia, and axial and oblique coronal images are better for detecting mandibular asymmetry. Features that can be observed are prominence of the upper lip with a small chin, subjective impression of a small or posteriorly displaced mandible, and a receding chin (Fig. 6). Measurements of the fetal mandible to provide data for the objective diagnosis of micrognathia have been reported [26,31,32]. Rotten [26] has defined two-dimensional and three-dimensional sonographic parameters for the objective diagnosis of retro- and micrognathia between 18 and 28 weeks' gestation. Associated clefting of the palate may be difficult to visualize unless the cleft extends to the alveolar margin [30].

Oculo–auriculo–vertebral spectrum

The oculo–auriculo–vertebral spectrum (OAVS) incorporates a variety of unilateral or bilateral and usually asymmetric disorders such as the first and second branchial arch syndrome, facio–auriculo–vertebral syndrome, hemifacial microsomia, and Goldenhar's syndrome. Hemifacial microsomia is the second most common craniofacial anomaly after CL/CP [33]. Disorders in the OAVS are characterized by facial asymmetry with mandibular hypoplasia that is usually unilateral but can be bilateral, with associated malformation of other first and sometimes second pharyngeal arch derivatives. Associated ear anomalies include microtia and stenosis or atresia of the external auditory canal. Orbital/ocular anomalies such as anophthalmia, microphthalmia, or orbital dystopia may be observed. In some cases there are additional anomalies of the brain, spine, heart, lungs, and genitourinary and gastrointestinal systems [34,35]. Goldenhar's syndrome has features of hemifacial microsomia with epibulbar dermoid and vertebral anomalies.

On fetal sonography the abnormal mandibular morphology with facial and mandibular hypoplasia, auricular asymmetry, and abnormal low placement of the pinna may be observed [36,37]. Sonographic imaging for auricular asymmetry and position is possible, but visualization of abnormal shape of the pinna is sometimes difficult [33]. Little has been written about fetal MR imaging in the diagnosis of micrognathia, and to date fetal MR imaging in the OAVS has not been reported. Theoretically, because

fetal MR imaging readily detects micrognathia, the asymmetry that is the hallmark of disorders within the OAVS spectrum could be apparent as well. Detection of cervical spinal fusion anomalies at present is cryptic with fetal MR imaging but can be well seen with ultrasound.

Abnormalities of the brain that can be associated with OAVS include hydrocephalus, Chiari I malformation, microcephaly, agenesis of the corpus callosum, and Dandy-Walker malformation [38]. Skeletal anomalies include scoliosis with vertebral and rib anomalies. The authors have observed clefting of the medulla and upper cervical cord in postnatal imaging of cases of Goldenhar's syndrome.

The differential diagnosis for OAVS, which is usually sporadic but can be inherited, includes the autosomal dominant Townes-Brock, branchio–oto–renal, and branchio–oculo–facial syndromes [33]. Townes-Brock syndrome is characterized by anal, ear, and thumb anomalies and, rarely, by mandibular asymmetry. Branchio–oto–renal syndrome resembles hemifacial microsomia, especially because the characteristic cervical fistulas, sinus tracts, and inner ear anomalies which would probably be cryptic on antenatal imaging. Branchio–oto–facial syndrome is characterized by cervical cutaneous defects, microphthalmia, nasolacrimal duct obstruction, abnormally shaped, low-set ears, and CL/CP. Prenatal diagnosis of this syndrome has not been reported, but the findings on prenatal sonography have been described [39].

Treacher Collins syndrome (mandibulofacial dysostosis)

Treacher Collins syndrome is an autosomal dominant disorder that results in symmetric micrognathia, retrognathia, facial underdevelopment, microtia, and atresia or stenosis of the external auditory canals. Additional anomalies include coloboma and CL/CP. Treacher Collins syndrome results from loss-of-function mutations in the gene TCOF1 that encodes for a nucleolar phosphoprotein known as treacle, which plays a crucial role in craniofacial development [40,41].

The characteristic features of micrognathia, canted palpebral fissures, and ear anomalies can be observed on prenatal imaging [42,43]. The diagnosis can be confirmed by prenatal screening for mutations in the Treacher Collins syndrome gene TCOF1 [44]. The differential diagnosis includes trisomy 18 and Nager's syndrome (acrofacial dysostosis), which resembles Treacher Collins syndrome with additional

limb anomalies such as short forearms, radioulnar synostosis, and hypoplasia or aplasia of the thumb or other digits. The diagnosis of Nager's syndrome has been made on antenatal sonography, based on the findings of severe micrognathia, malformed ears with preauricular tags, mesomelic limb shortening, absence of one thumb and absence of the contralateral second finger, and following the exclusion of trisomy 18 by karyotyping [45]. Nager's syndrome has also been imaged in the fetus with MR (Fig. 6).

Robin sequence

The Robin sequence consists of CP, glossoptosis secondary to micrognathia, respiratory distress, and feeding issues. Retrognathia can also occur. It has been postulated that early mandibular hypoplasia results in posterior displacement of the tongue, preventing normal palatal development and fusion and resulting in a U-shaped CP [29]. This sequence of events has been validated in a murine model [46]. The Robin sequence is etiologically heterogeneous and can be sporadic or part of a number of different syndromes. The most common of these is the autosomal dominant Stickler syndrome, accounting for approximately 30% to 40% of syndromic causes of the Robin sequence [47]. Stickler syndrome is a connective tissue disorder with features including myopia, vitreoretinal degeneration, joint hypermobility, premature osteoarthropathy, mild spondyloepiphyseal dysplasia, hearing loss, and the Pierre-Robin sequence [48,49]. The majority of patients with Stickler syndrome have mutations in the gene encoding type II collagen (*COL2A1*) on chromosome 12q13 [49]. Velocardiofacial syndrome is the second most common syndrome associated with the Robin sequence and accounts for approximately 17% of cases. Ten percent of patients with velocardiofacial syndrome have the DiGeorge sequence [33]. The syndrome is characterized by CP, cardiac anomalies, typical facies, and learning disabilities [50]. Patients with velocardiofacial syndrome or DiGeorge sequence often have a deletion if chromosome 22q11 that is detectable by fluorescence in situ hybridization [51].

Prenatal sonographic features of the Robin sequence include micrognathia, polyhydramnios, and CP [52,53].

Ocular and orbital abnormalities

Standardized measurements of interorbital and binocular distance permit antenatal diagnosis of both hypotelorism and hypertelorism [1–3]. Malformations associated with hypertelorism include a variety of chromosomal aberrations including Turner's syn-
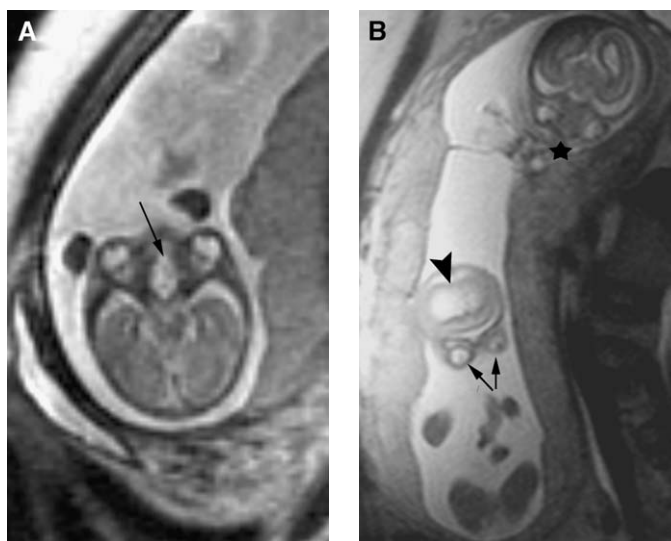

Fig. 7. (*A*) Hypertelorism in a fetus imaged with MR at 21.5 weeks' gestation. This axial SSFSE T2-weighted image also reveals a fluid-filled cephalocele between the orbits (see also Fig. 4). (*B*) Hypotelorism in one fetus of a dichorionic, diamniotic twin gestation. A coronal SSFSE T2-weighted MR image of the nonpresenting twin reveals hypotelorism (*arrows*). There is a monoventricle (*arrowhead*) consistent with holoprosencephaly. Compare the interocular distance with the normal presenting twin (*star*). (Courtesy of D. Levine, MD, Boston, MA.)

drome, frontonasal malformation, craniofrontonasal syndrome, paramedian facial clefts, encephalocele, and many other entities and syndromes (Fig. 7A) [54].

Hypotelorism is associated with holoprosencephaly (of various causes), trisomy 13, trisomy 21, and a variety of other disorders and chromosomal anomalies (Fig. 7B). The detection of hypotelorism associated with trisomy 13 has been reported based on ocular biometric parameters obtained with transvaginal sonography during the first half of pregnancy [1].

Fetal ocular development has been assessed with fetal MR imaging with the establishment of a linear model of ocular growth curve in utero [55]. Evaluation of ocular development may allow the detection and confirmation of ocular anomalies such as microphthalmia. Microphthalmia is a feature of numerous conditions and is frequently seen with triploidy, trisomy 13, Aicardi's syndrome, CHARGE (coloboma of the eye, choanal atresia, retardation, and genital and ear anomalies) association, frontonasal dysplasia sequence, and Walker-Warburg syndrome [56]. Microphthalmia can manifest as a small globe with or without associated orbital cysts.

Craniosynostosis

Premature fusion of the cranial sutures or craniosynostosis can affect one or multiple sutures, leading to cranial and sometimes orbital deformation. Craniosynostosis can be syndromic or nonsyndromic, sporadic or inherited. A prenatal diagnosis of craniosynostosis carries significant cosmetic and surgical implications, depending on the ultimate phenotypic or genetic diagnosis. Although cranial sutures can be visualized by three-dimensional sonography as early as 13 weeks' gestation, a diagnosis of fetal craniosynostosis is usually made based on secondary features such as cranial deformation and, in some cases, hypertelorism or hypotelorism [33].

Premature fusion of a single coronal (frontoparietal and frontosphenoid) suture results in ipsilateral cranial flattening or plagiocephaly with elevation and posterior displacement of the ipsilateral orbit and anterior displacement of the ipsilateral ear canal. The sonographic finding of unilateral coronal synostosis diagnosed retrospectively in a fetal sonogram obtained at approximately 21.5 weeks' gestation has been described [57]. Premature fusion of a single lambdoid suture is less common and produces parieto-occipital plagiocephaly.

Synostosis of the sagittal suture results in a decrease in the biparietal diameter of the calvarium and an increase in anteroposterior dimension with scaphocephaly or dolichocephaly. Sagittal synostosis is variable in onset and can occur from the late first trimester to the early postnatal period [33]. Sagittal synostosis can affect only a segment or the whole length of the suture and may be isolated or occur in association with premature fusion of other sutures. Similarly the cause is variable.

Premature fusion of the metopic suture results in a triangular shape of the anterior cranium, sometimes termed trigonocephaly. The abnormal shape of the skull can be detected by fetal sonography and MR imaging, which demonstrate bitemporal narrowing and sometimes hypotelorism (Fig. 8). Metopic synostosis is nonsyndromic in approximately 72% to 75% of cases, affects males more commonly than females, and is usually sporadic but can be familial [58,59]. Syndromic forms can occur in association with chromosomal as well as single-gene disorders [58]. Fetal exposure to sodium valproate is also associated with metopic synostosis [59].

Craniosynostosis of both coronal sutures results in brachycephaly or turribrachycephaly with a relative reduction in anteroposterior dimension of the calvarium. Bilateral coronal synostosis with or without fusion of other sutures is a feature of a number of syndromes, as outlined later. Fusion of coronal and lambdoid sutures produces Kleeblattschädel, or cloverleaf deformity of the skull, with bitemporal and bifrontal bulging (Fig. 9). This morphology has been most frequently observed in thanatophoric dwarfism, but can be a feature of the Pfeiffer's, Apert's and Crouzon's syndromes [33,57,60].

Antenatal diagnosis of syndromic craniosynostosis can be made based on cranial dysmorphology [61–63]. In a retrospective review of patients with a known postnatal diagnosis of craniosynostosis, Miller et al [57] were not able to diagnose craniosynostosis on sonography obtained during the first trimester. Using indirect features of cranial deformity (Kleeblattschädel, brachycephaly, and trigonocephaly), however, these authors were able to diagnose craniosynostosis in a proportion of patients during the second and third trimesters.

Phenotypic designation is not always possible unless there is a known family history or characteristic limb deformities as seen in Apert's, Pfeiffer's, and Carpenter's syndromes. In addition, the craniosynostosis syndromes are clinically heterogeneous with overlapping features, which sometimes preclude accurate phenotypic diagnosis. Prenatal or postnatal molecular diagnosis can also be obtained [64,65]. Crouzon's, Apert's, and Pfeiffer's syndromes have been linked to a number of fibroblast growth factor receptor mutations [64]. Saethre-Chotzen syndrome
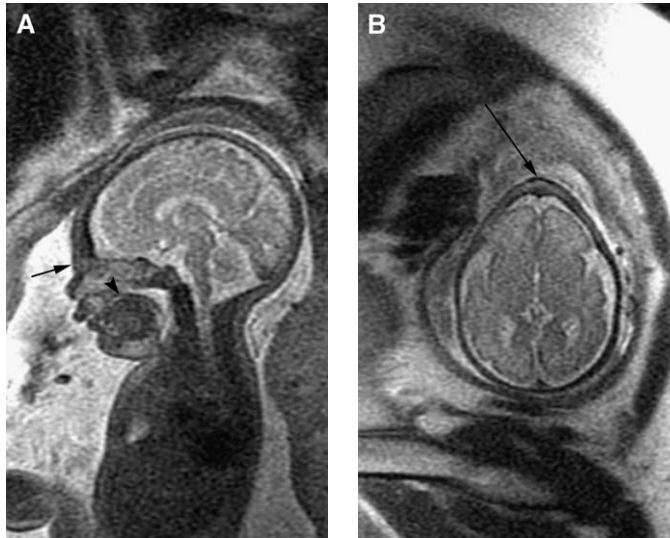
Fig. 8. Metopic synostosis diagnosed by MR in a fetus imaged at 30 weeks' gestation, and also found to have dextroposition of the fetal heart and absent radii. (*A*) Sagittal SSFSE T2-weighted image reveals an abnormal profile. There is abnormal bony thickening of the inferior aspect of the frontal bone (*arrow*). There is mild micrognathia and an abnormally high-arched palate (*arrowhead*). (*B*) The axial image demonstrates trigonocephaly consistent with premature fusion of the metopic suture (*arrow*). This constellation of findings is suggestive of Baller-Gerold syndrome. Further testing for the TWIST mutation associated with this disorder is pending [89,90].

is caused by mutations or deletions in the *TWIST* gene that may function as an upstream regulator of fibroblast growth factor receptors [66,67].

A diagnosis of syndromic craniosynostosis has significant implications in terms of parental counseling. There is often severe cosmetic abnormality (cranial deformity, midfacial hypoplasia, exorbitism), and multiple surgical procedures, such as craniotomy and midfacial advancement, can be anticipated. In addition ventriculostomy may be required to alleviate hydrocephalus, and sometimes posterior fossa decompression is performed for treatment of Chiari I malformation and hydrosyringomyelia (Fig. 9). Compromise of the airway sometimes necessitates endotracheal intubation or tracheostomy. Abnormalities of the hands and feet will also require surgical correction.

Crouzon's syndrome

Patients with Crouzon's syndrome have bilateral coronal ring sutural fusion and sometimes synostosis of other sutures. In addition to cranial deformity, there is exorbitism with mild hypertelorism that can be observed during the third trimester [68]. In familial cases, the diagnosis can be established by imaging during the second trimester based on progressive in-

crease in the binocular and interorbital measurements [69]. Ventriculomegaly is sometimes also observed.

Apert's syndrome

The typical features of Apert's syndrome include brachycephaly or turribrachycephaly and symmetric syndactyly of the hands and feet. In Apert's syndrome, unlike Crouzon's syndrome, the metopic suture, anterior fontanel, and, sometimes, the sagittal suture are usually widely patent. Apert's syndrome is usually diagnosed sonographically during the third trimester, can be diagnosed during the second trimester, and has been associated with a mittenlike deformity of the hand observed during the first trimester [62,63,70]. Other features include ventriculomegaly and a high-arched palate or CP. Spinal fusion anomalies may be difficult to detect antenatally. Midnasal stenosis and midfacial hypoplasia contribute to narrowing of the airway during the neonatal period or later in childhood.

Pfeiffer's syndrome

The cranial deformities in Pfeiffer's syndrome, and exorbitism resemble Crouzon's syndrome. A
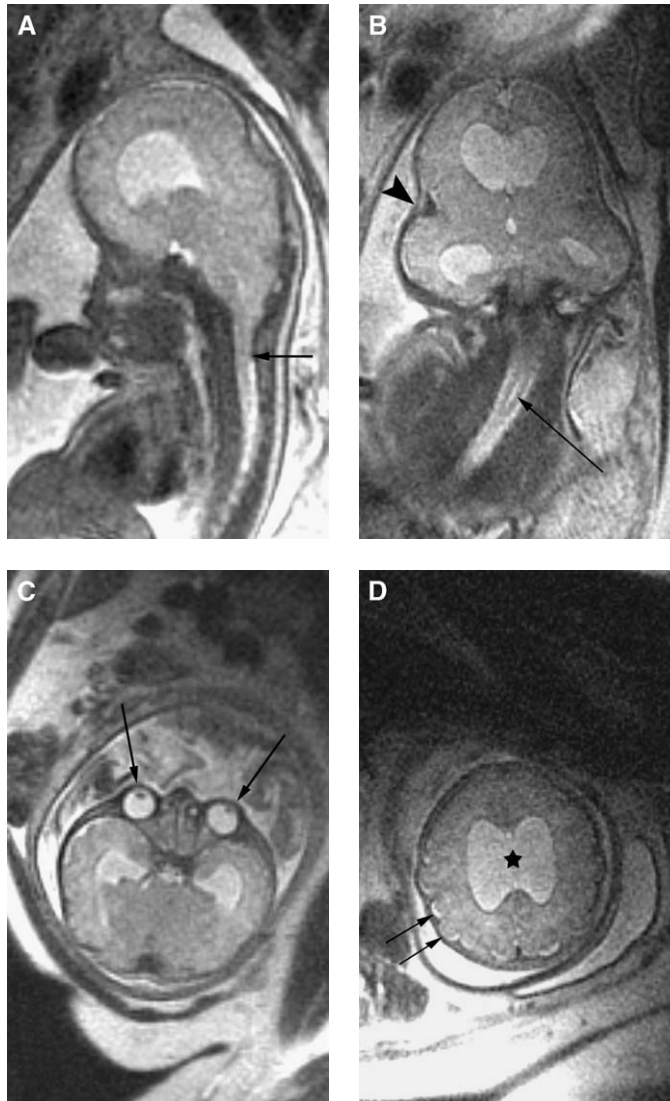
Fig. 9. Kleeblattschädel diagnosed in a male fetus imaged with MR at 37.5 weeks' gestation. (*A*) Sagittal SSFSE T2-weighted image demonstrates turricephaly and shortening of the anterior cranial fossa. The ventricles are dilated. The occiput is flattened, and the posterior fossa is small. There is herniation of the cerebellar tonsils (*arrow*) beyond the foramen magnum consistent with a Chiari I malformation. (*B*) Coronal image demonstrates brachycephaly with an indentation in the region of the fused squamosal sutures (*arrow*). There is ventriculomegaly and hydrosyringomyelia (*arrow*). (*C*) Axial image reveals brachycephaly and exorbitism (arrows) caused by coronal ring synostosis. (*D*) A more cephalad axial image reveals prominent convolutional impressions on the calvarium (*arrows*) and ventriculomegaly (*star*). These features are consistent with syndromic craniosynostosis with synostosis of multiple sutures that was confirmed following delivery of the baby. The hands of the infant appear normal. The phenotypic diagnosis is uncertain, and the genetic diagnosis is pending. The baby has undergone surgical release of cranial sutures, ventriculoperitoneal shunting, and posterior fossa decompression.

distinctive but not invariable feature of Pfeiffer's syndrome is broad, medially rotated thumbs and varus deformity of the great toes. Antenatal sonographic detection of the cranial deformity and abnormalities of the digits has been reported [61,71,72].

Carpenter's syndrome

Craniosynostosis, polydactyly, brachydactyly, variable soft-tissue syndactyly, and cardiac defects characterize Carpenter's syndrome, which has been diagnosed on antenatal sonography [73].

Posterior nuchal translucency

Posterior nuchal translucency or nuchal thickness refers to a sonographic measurement of nuchal skin and subcutaneous tissue measured on a standardized sub-occipito-bregmatic view. Nuchal thickness increases with advancing gestational age in the chromosomally normal population. Causes of increased

Fig. 10. MR image of twin pregnancy at 19.5 weeks' gestation. There is severe hydrops fetalis of the presenting breech twin, which has diffuse abnormal thickening and lucency of the subcutaneous tissues (*long arrow*). There is also fetal ascites (*short arrow*). There is a cystic mass within the subcutaneous tissues of the neck (*arrowhead*) consistent with lymphatic fluid accumulation that occurs in Turner's syndrome. The brain appears hypointense because of infarction from fetal demise. Chromosomal analysis confirmed an XO karyotype consistent with a diagnosis of Turner's syndrome in the affected twin.

width of nuchal translucency include redundant nuchal skin, nuchal edema, lymphedema, and, sometimes, lymphatic malformations. Increased posterior nuchal translucency between 10 to 14 weeks' gestation is associated with increased risk of fetal aneuploidy, and this risk increases with both maternal age and thickness of nuchal translucency [74]. Trisomies 21, 18, and 13, Turner's syndrome (XO), and triploidy are all associated with increased width of nuchal translucency. Therefore increased nuchal translucency detected during the first trimester should warrant offering fetal karyotyping [74]. In Turner's syndrome, subcutaneous accumulation of fluid occurs in the neck region and can be visualized sonographically from 10 to 14 weeks of gestation as massively increased nuchal translucency. Septations within the fluid accumulation and cystic accumulations of fluid also occur and are sometimes termed lymphatic malformation or cystic hygroma (Fig. 10). In fetuses with Turner's syndrome, this phenomenon has been linked to hypoplastic lymphatic vessels in the upper dermis [75].

Cephaloceles

Cephaloceles are discussed in detail elsewhere is this issue. Cephalocele is characterized by a midline sac containing cerebrospinal fluid or tissue, associated with a defect of the calvarium or skull base (see Figs. 4, 7). A neuroglial heterotopia (nasal glioma) resembles a cephalocele but lacks a communication with the intracranial contents. In assessing a fetus with hypertelorism, one should evaluate the integrity of the anterior skull base and the interorbital soft tissues for possible cephalocele. The brain should be carefully evaluated for associated findings such as agenesis of the corpus callosum, pericallosal lipomas, interhemispheric cyst, and cortical malformation. Cystic masses that may be mistaken for cephaloceles include nasolacrimal duct cysts, lymphatic malformations, teratoma, and hemangioma. Nasolacrimal duct cyst is associated with an intact skull base and is located adjacent to the medial aspect of the globe with a tubular fluid-filled structure that extends to beneath the inferior nasal turbinate.

Tumors and vascular anomalies

Fetal scalp or neck masses may be detected on routine antenatal sonography. Fetal MR imaging provides further information regarding the extent of the lesion, local mass effect, and associated abnor-

malities. Imaging characteristics that assist in determining a likely diagnosis include the location and vascularity of the mass and whether the lesion is solid, cystic, or both. The fluid-filled pharynx and trachea should be assessed for distortion or compression by the mass. This information permits parental counseling with regard to the strategy for delivery and the most likely diagnosis or differential diagnoses. Compression of the fetal airway requires intensive maternal–fetal monitoring. Subsequent delivery often warrants specialized delivery by cesarean section with maximal uterine relaxation and maintenance of intact feto-placental circulation while the airway is secured [76]. This procedure is termed ex utero intrapartum treatment or the EXIT procedure. The most commonly encountered fetal masses are vascular anomalies (eg, hemangioma and lymphatic malformation) and teratoma.

Vascular anomalies

Vascular anomalies manifest as either vascular tumors or vascular malformations. The commonest vascular tumor is hemangioma. Although hemangiomas typically appear postnatally around 2 weeks of age, true congenital hemangiomas that develop in the fetus have been described [77,78]. Common postnatal hemangiomas usually proliferate during the first year of life and then involute, with slow regression during the several ensuing years. Congenital hemangiomas tend to grow in utero but have been observed to stabilize during the third trimester. Postnatally, a proportion of congenital hemangiomas involutes more rapidly than the common postnatal hemangiomas [78]. Some congenital hemangiomas, however, do not regress postnatally and persist into late childhood [79]. Histologically, these two types of uncommon congenital hemangioma have some clinical and pathologic features that overlap with the common infantile hemangioma, but microscopic architectural differences between the three types of hemangioma have also been observed [80].

Fetal hemangioma has been detected as early as 12 weeks' gestation [78]. The impact of the hemangioma on the fetus depends on the size and location, associated anomalies, if present, and complications such as mass effect on the fetal airway, cardiac failure, and polyhydramnios. Scalp hemangiomas may ulcerate with resultant alopecia [77]. If indicated, maternal steroids can be administered to accelerate involution of the hemangioma. If there is compression of the airway, delivery of the fetus by caesarian section with endotracheal intubation while on placental support is optimal [81].

Involuting congenital hemangioma can be easily diagnosed and involutes rapidly (Fig. 11). Regression
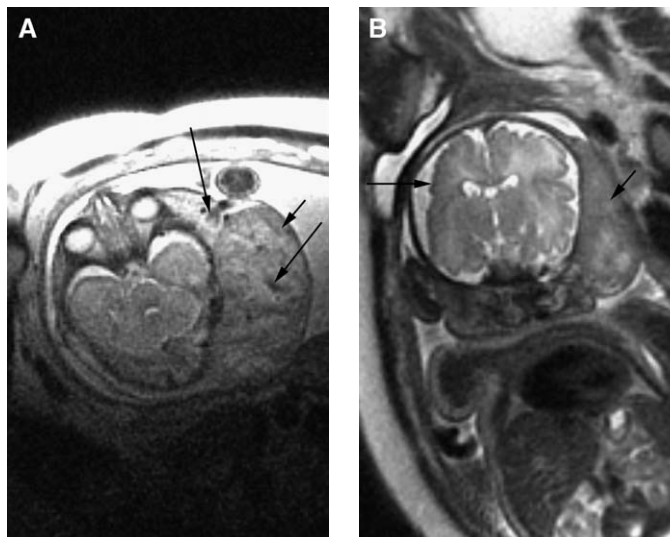

Fig. 11. A scalp mass imaged with MR in a fetus at 35 weeks' gestation. (*A*) Axial SSFSE T2-weighted MR image reveals a large, mildly heterogeneous left scalp mass (short arrow) that is isointense with brain. Serpiginous flow voids are present in and adjacent to the mass indicating enlarged vessels (*long arrows*). (*B*) Coronal image reveals the mass (*short arrow*) and polymicrogyria involving the contralateral cerebral hemisphere (*long arrow*). At the time of initial imaging, a diagnosis of probable hemangioma was made, with a differential diagnosis of congenital fibrosarcoma. The mass was observed to stabilize in size and by birth had commenced involution consistent with congenital hemangioma.

usually occurs by 12 to 14 months of age, sometimes leaving residua such as atrophic skin and subcutaneous tissue or large veins. Postnatal surgical intervention may be indicated to alleviate ulceration, bleeding, visual obstruction, and occasionally arteriovenous shunting resulting in congestive cardiac failure or for cosmetic reasons [80]. The imaging features of noninvoluting congenital hemangioma may be confused with those of congenital fibrosarcoma [82]. The acronym PHACES has been proposed to emphasize the association of the following characteristic features: *p*osterior fossa malformations, *h*emangiomas, *a*rterial anomalies, *c*oarctation of the aorta and *c*ardiac defects, *e*ye abnormalities, and *s*ternal malformations [83,84]. There have also been reports of cortical malformation associated with hemangioma [85–87]. Although these reports deal chiefly with postnatal hemangioma, the authors have observed polymicrogyria in association with congenital hemangioma.

On antenatal sonography, congenital hemangioma appears as a large, solid, heterogeneous, vascular mass, with prominent arterial and venous flow. Enlargement of the ipsilateral carotid artery and internal jugular vein may also be observed with craniofacial hemangiomas. On MR imaging, hemangioma appears as a sharply circumscribed solid, somewhat heterogeneous tumor with signal intensity ranging from isointense with gray matter to isointense with white matter (Fig. 11). Flow voids indicating prominent vascularity may also be observed. The brain should be carefully assessed for associated arterial anomalies and cortical malformation (Fig. 11B).

The most commonly diagnosed fetal vascular malformation is lymphatic malformation, a lesion that consists of localized or diffuse dysplastic lymphatic channels and cysts. Terms such as cystic hygroma and lymphangioma, although commonly used to describe this entity, are thought to contribute to diagnostic confusion and are regarded as outdated [77]. Lymphatic malformations may contain large cystic spaces (macrocystic), subcentimeter cystic spaces (microcystic), or a combination. Turner's syndrome, or gonadal dysgenesis, has been associated with both increased posterior nuchal thickness and large septated cystic masses that have been attributed to hypoplastic lymphatic vessels in the upper dermis (see Fig. 10) [75].

Sonographic examination of lymphatic malformation reveals a cystic, anechoic, septated mass that must be differentiated from a predominantly cystic teratoma and other developmental cystic abnormalities such as cephaloceles, salivary duct cysts, foregut duplication cysts, and thymic cysts. Lymphatic mal-

Fig. 12. A neck mass diagnosed shortly by birth in a fetus imaged at 38 weeks' gestation. MR imaging was obtained to determine patency of the fetal airway. Coronal SSFSE T2-weighted MR image reveals a cystic mass involving the left side of the neck. The mass contains septations (*arrow*). Lymphatic malformation was diagnosed and confirmed following delivery.

formation must also be differentiated and distinguished from posterior nuchal translucency seen during the early first and second trimester. In this regard the term cystic hygroma has been confusingly and erroneously used to describe both entities.

On MR imaging of the fetus, lymphatic malformations appear septated and markedly hyperintense on T2-weighted images (Fig. 12). Lymphatic malformations are usually diagnosed antenatally during the second or third trimester, in contrast to first-trimester diagnosis of nuchal translucency [77].

Antenatal detection of lymphatic malformation allows for careful planning of delivery to secure and protect the airway of the infant during delivery. One of the commonest complications of lymphatic malformation is hemorrhage, often in response to minimal trauma. This propensity may also affect the strategy for delivery.

Teratoma

Teratomas are the most common congenital tumors. The head and neck region is the second most common location for teratomas in early infancy, after sacrococcygeal location. Antenatal diagnosis of teratoma can be made with fetal sonography or MR imaging. Demonstration of airway compression by
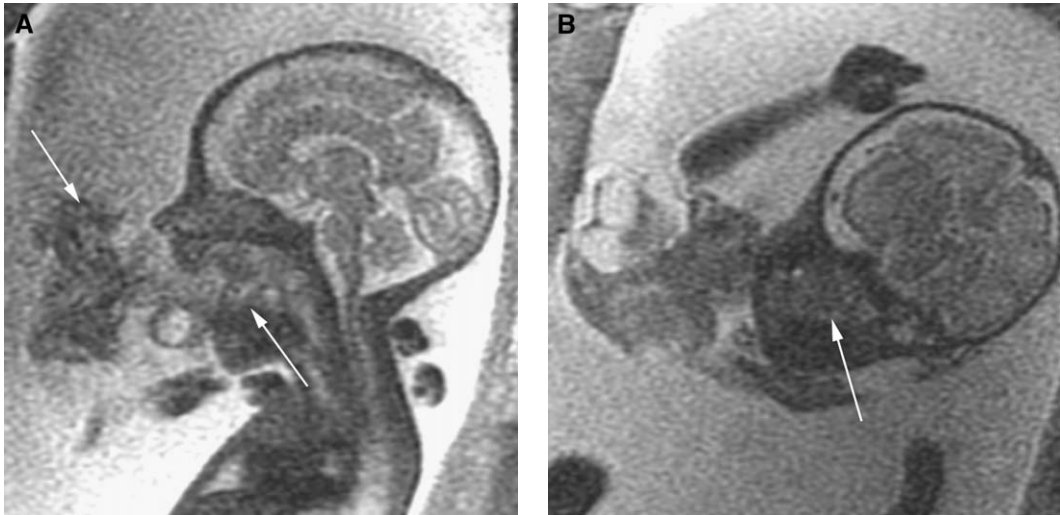
Fig. 13. A neck mass imaged with MR imaging at 31 weeks' gestation. (*A*) Sagittal SSFSE T2-weighted image reveals a heterogeneous solid and cystic mass (*arrows*) located within and expanding the oral cavity. The tumor extrudes out of the mouth into the surrounding amniotic fluid. The hard palate could not be identified, and a palatal cleft was suspected. (*B*) Coronal image demonstrates that there is a deep component that extends beyond the confines of the oral cavity. The tumor was diagnosed as a teratoma with obstruction of the upper airway. Elective cesarean section was performed with delivery of the baby by the EXIT procedure. The tumor has been resected with histologic confirmation of teratoma. A wide cleft of the hard palate was present in the baby girl and was thought to result from the prevention of normal palatal development by the tumor.

the teratoma is likely to affect the timing and mode of delivery. An EXIT delivery may be life saving in these cases [88]. On fetal sonography and MR imaging, teratomas appear heterogeneous but sharply circumscribed, with solid and cystic areas (Fig. 13). Compression of the airway can occur at any level. Because the normal airway is usually fluid filled on MR imaging, lack of the normal fluid column within the pharynx or trachea may provide an indirect sign of airway compression. Midline teratoma that involves the oral cavity can be associated with CP deformity (Fig. 13). Fetal MR imaging also provides useful information about the extent of the tumor toward the skull base, into deep fascial compartments of the neck, and into the mediastinum. The differential diagnosis for predominantly cystic teratoma includes lymphatic malformation and foregut duplication cyst. Less common solid tumors in the fetus include rhabdomyoma and congenital infantile fibrosarcoma.

Summary

The imaging of fetal head and neck anomalies is a rapidly evolving and developing phenomenon. Fetal MR imaging has recently emerged as a useful and complementary imaging modality beyond the first few months of pregnancy. Novel discoveries about the genetic and molecular mechanisms of disease and the vast amount of literature now widely available on the Internet provide an incentive for self-education for all radiologists involved in fetal imaging. This education, in turn, may lead to improved diagnostic accuracy and will significantly affect parental counseling and subsequent management of pregnancy and delivery.

References

[1] Rosati P, Guariglia L. Early transvaginal fetal orbital measurements: a screening tool for aneuploidy? J Ultrasound Med 2003;22:1201–5.

[2] Trout T, Budorick NE, Pretorius DH, et al. Significance of orbital measurements in the fetus. J Ultrasound Med 1994;13:937–43.

[3] Mayden KL, Tortora M, Berkowitz RL, et al. Orbital diameters: a new parameter for prenatal diagnosis and dating. Am J Obstet Gynecol 1982;144:289–97.

[4] Cash C, Set P, Coleman N. The accuracy of antenatal ultrasound in the detection of facial clefts in a low-risk screening population. Ultrasound Obstet Gynecol 2001; 18:432–6.

[5] Walker SJ, Ball RH, Babcook CJ, et al. Prevalence of aneuploidy and additional anatomic abnormalities in fetuses and neonates with cleft lip with or without

cleft palate: a population-based study in Utah. J Ultrasound Med 2001;20:1175–80.

[6] Online Mendelian Inheritance in Man. OMIM. McKusick-Nathans Institute for Genetic Medicine, Johns Hopkins University (Baltimore, MD) and National Center for Biotechnology Information, National Library of Medicine (Bethesda, MD), 2000. Available at: http://www.ncbi.nlm.nih.gov/omim/. Accessed February 2004.

[7] Stoll C, Alembik Y, Dott B, et al. Associated malformations in cases with oral clefts. Cleft Palate Craniofac J 2000;37:41–7.

[8] Saltzman DH, Benacerraf BR, Frigoletto FD. Diagnosis and management of fetal facial clefts. Am J Obstet Gynecol 1986;155:377–9.

[9] Berge SJ, Plath H, Van de Vondel PT, et al. Fetal cleft lip and palate: sonographic diagnosis, chromosomal abnormalities, associated anomalies and postnatal outcome in 70 fetuses. Ultrasound Obstet Gynecol 2001; 18:422–31.

[10] Ghi T, Tani G, Savelli L, et al. Prenatal imaging of facial clefts by magnetic resonance imaging with emphasis on the posterior palate. Prenat Diagn 2003;23: 970–5.

[11] Mulliken JB, Benacerraf BR. Prenatal diagnosis of cleft lip: what the sonologist needs to tell the surgeon. J Ultrasound Med 2001;20:1159–64.

[12] Nyberg DA, Hegge FN, Kramer D, et al. Premaxillary protrusion: a sonographic clue to bilateral cleft lip and palate. J Ultrasound Med 1993;12:331–5.

[13] Nyberg DA, Sickler GK, Hegge FN, et al. Fetal cleft lip with and without cleft palate: US classification and correlation with outcome. Radiology 1995;195: 677–84.

[14] Robinson JN, McElrath TF, Benson CB, et al. Prenatal ultrasonography and the diagnosis of fetal cleft lip. J Ultrasound Med 2001;20:1165–70.

[15] Ghi T, Perolo A, Banzi C, et al. Two-dimensional ultrasound is accurate in the diagnosis of fetal craniofacial malformation. Ultrasound Obstet Gynecol 2002; 19:543–51.

[16] Pilu G, Reece EA, Romero R, et al. Prenatal diagnosis of craniofacial malformations with ultrasonography. Am J Obstet Gynecol 1986;155:45–50.

[17] Monni G, Ibba RM, Olla G, et al. Color Doppler ultrasound and prenatal diagnosis of cleft palate. J Clin Ultrasound 1995;23:189–91.

[18] Levine D. Prenatal diagnosis of cleft lip and cleft palate by magnetic resonance imaging: a pictorial essay. AJR Am J Roentgenol 2004, in press.

[19] Tessier P. Anatomical classification facial, craniofacial and latero-facial clefts. J Maxillofac Surg 1976; 4:69–92.

[20] Cohen Jr MM. Asymmetry: molecular, biologic, embryopathic, and clinical perspectives. Am J Med Genet 2001;101:292–314.

[21] Kawamoto Jr HK. The kaleidoscopic world of rare craniofacial clefts: order out of chaos (Tessier classification). Clin Plast Surg 1976;3:529–72.

[22] Taub PJ, Bradley JP, Setoguchi Y, et al. Typical facial clefting and constriction band anomalies: an unusual association in three unrelated patients. Am J Med Genet 2003;120A:256–60.

[23] Orioli IM, Ribeiro MG, Castilla EE. Clinical and epidemiological studies of amniotic deformity, adhesion, and mutilation (ADAM) sequence in a South American (ECLAMC) population. Am J Med Genet 2003;118A: 135–45.

[24] Stanek J, de Courten-Myers G, Spaulding AG, et al. Case of complex craniofacial anomalies, bilateral nasal proboscides, palatal pituitary, upper limbs reduction, and amnion rupture sequence: disorganization phenotype? Pediatr Dev Pathol 2001;4:192–202.

[25] Huppert BJ, Brandt KR, Ramin KD, et al. Single-shot fast spin-echo MR imaging of the fetus: a pictorial essay [special issue]. Radiographics 1999;19: S215–27.

[26] Rotten D, Levaillant JM, Martinez H, et al. The fetal mandible: a 2D and 3D sonographic approach to the diagnosis of retrognathia and micrognathia. Ultrasound Obstet Gynecol 2002;19:122–30.

[27] Nicolaides KH, Salvesen DR, Snijders RJ, et al. Fetal facial defects: associated malformations and chromosomal abnormalities. Fetal Diagn Ther 1993;8:1–9.

[28] Bromley B, Benacerraf BR. Fetal micrognathia: associated anomalies and outcome. J Ultrasound Med 1994;13:529–33.

[29] Hanson JW, Smith DW. U-shaped palatal defect in the Robin anomalad: developmental and clinical relevance. J Pediatr 1975;87:30–3.

[30] Vettraino IM, Lee W, Bronsteen RA, et al. Clinical outcome of fetuses with sonographic diagnosis of isolated micrognathia. Obstet Gynecol 2003;102: 801–5.

[31] Watson WJ, Katz VL. Sonographic measurement of the fetal mandible: standards for normal pregnancy. Am J Perinatol 1993;10:226–8.

[32] Paladini D, Morra T, Teodoro A, et al. Objective diagnosis of micrognathia in the fetus: the jaw index. Obstet Gynecol 1999;93:382–6.

[33] Wong GB, Mulliken JB, Benacerraf BR. Prenatal sonographic diagnosis of major craniofacial anomalies. Plast Reconstr Surg 2001;108:1316–33.

[34] Cohen Jr MM, Rollnick BR, Kaye CI. Oculoauriculovertebral spectrum: an updated critique. Cleft Palate J 1989;26:276–86.

[35] Rollnick BR, Kaye CI, Nagatoshi K, et al. Oculoauriculovertebral dysplasia and variants: phenotypic characteristics of 294 patients. Am J Med Genet 1987;26: 361–75.

[36] Benacerraf BR, Frigoletto Jr FD. Prenatal ultrasonographic recognition of Goldenhar's syndrome. Am J Obstet Gynecol 1988;159:950–2.

[37] Tamas DE, Mahony BS, Bowie JD, et al. Prenatal sonographic diagnosis of hemifacial microsomia (Goldenhar-Gorlin syndrome). J Ultrasound Med 1986;5: 461–3.

[38] Horgan JE, Padwa BL, LaBrie RA, et al. OMENS-

Plus: analysis of craniofacial and extracraniofacial anomalies in hemifacial microsomia. Cleft Palate Craniofac J 1995;32:405–12.

[39] Bromley B, Miller WA, Mansour R, et al. Prenatal findings of branchio-oculo-facial syndrome. J Ultrasound Med 1998;17:475–7.

[40] Dixon J, Brakebusch C, Fassler R, et al. Increased levels of apoptosis in the prefusion neural folds underlie the craniofacial disorder, Treacher Collins syndrome. Hum Mol Genet 2000;9:1473–80.

[41] The Treacher Collins Syndrome Collaborative Group. Positional cloning of a gene involved in the pathogenesis of Treacher Collins syndrome. Nat Genet 1996;12: 130–6.

[42] Meizner I, Carmi R, Katz M. Prenatal ultrasonic diagnosis of mandibulofacial dysostosis (Treacher Collins syndrome). J Clin Ultrasound 1991;19:124–7.

[43] Cohen J, Ghezzi F, Goncalves L, et al. Prenatal sonographic diagnosis of Treacher Collins syndrome: a case and review of the literature. Am J Perinatol 1995;12:416–9.

[44] Ellis PE, Dawson M, Dixon MJ. Mutation testing in Treacher Collins syndrome. J Orthod 2002;29:293–7 [discussion: 278].

[45] Paladini D, Tartaglione A, Lamberti A, et al. Prenatal ultrasound diagnosis of Nager syndrome. Ultrasound Obstet Gynecol 2003;21:195–7.

[46] Ricks JE, Ryder VM, Bridgewater LC, et al. Altered mandibular development precedes the time of palate closure in mice homozygous for disproportionate micromelia: an oral clefting model supporting the Pierre-Robin sequence. Teratology 2002;65:116–20.

[47] Sheffield LJ, Reiss JA, Strohm K, et al. A genetic follow-up study of 64 patients with the Pierre Robin complex. Am J Med Genet 1987;28:25–36.

[48] Stickler GB, Hughes W, Houchin P. Clinical features of hereditary progressive arthro-ophthalmopathy (Stickler syndrome): a survey. Genet Med 2001;3:192–6.

[49] Snead MP, Yates JR. Clinical and molecular genetics of Stickler syndrome. J Med Genet 1999;36:353–9.

[50] Shprintzen RJ, Goldberg RB, Lewin ML, et al. A new syndrome involving cleft palate, cardiac anomalies, typical facies, and learning disabilities: velo-cardio-facial syndrome. Cleft Palate J 1978;15:56–62.

[51] Gong W, Emanuel BS, Collins J, et al. A transcription map of the DiGeorge and velo-cardio-facial syndrome minimal critical region on 22q11. Hum Mol Genet 1996;5:789–800.

[52] Soulier M, Sigaudy S, Chau C, et al. Prenatal diagnosis of Pierre-Robin sequence as part of Stickler syndrome. Prenat Diagn 2002;22:567–8.

[53] Hsieh YY, Chang CC, Tsai HD, et al. The prenatal diagnosis of Pierre-Robin sequence. Prenat Diagn 1999;19:567–9.

[54] Tan ST, Mulliken JB. Hypertelorism: nosologic analysis of 90 patients. Plast Reconstr Surg 1997;99: 317–27.

[55] Bremond-Gignac DS, Benali K, Deplus S, et al. In utero eyeball development study by magnetic resonance imaging. Surg Radiol Anat 1997;19:319–22.

[56] Jones KL. Smith's recognizable patterns of human malformation. Philadelphia: W.B. Saunders; 1997.

[57] Miller C, Losken HW, Towbin R, et al. Ultrasound diagnosis of craniosynostosis. Cleft Palate Craniofac J 2002;39:73–80.

[58] Azimi C, Kennedy SJ, Chitayat D, et al. Clinical and genetic aspects of trigonocephaly: a study of 25 cases. Am J Med Genet 2003;117A:127–35.

[59] Lajeunie E, Barcik U, Thorne JA, et al. Craniosynostosis and fetal exposure to sodium valproate. J Neurosurg 2001;95:778–82.

[60] Stamm ER, Pretorius DH, Rumack CM, et al. Kleeblattschadel anomaly. In utero sonographic appearance. J Ultrasound Med 1987;6:319–24.

[61] Benacerraf BR, Spiro R, Mitchell AG. Using three-dimensional ultrasound to detect craniosynostosis in a fetus with Pfeiffer syndrome. Ultrasound Obstet Gynecol 2000;16:391–4.

[62] Pooh RK, Nakagawa Y, Pooh KH, et al. Fetal craniofacial structure and intracranial morphology in a case of Apert syndrome. Ultrasound Obstet Gynecol 1999; 13:274–80.

[63] Skidmore DL, Pai AP, Toi A, et al. Prenatal diagnosis of Apert syndrome: report of two cases. Prenat Diagn 2003;23:1009–13.

[64] Mulliken JB, Steinberger D, Kunze S, et al. Molecular diagnosis of bilateral coronal synostosis. Plast Reconstr Surg 1999;104:1603–15.

[65] Schwartz M, Kreiborg S, Skovby F. First-trimester prenatal diagnosis of Crouzon syndrome. Prenat Diagn 1996;16:155–8.

[66] Howard TD, Paznekas WA, Green ED, et al. Mutations in TWIST, a basic helix-loop-helix transcription factor, in Saethre-Chotzen syndrome. Nat Genet 1997; 15:36–41.

[67] el Ghouzzi V, Le Merrer M, Perrin-Schmitt F, et al. Mutations of the TWIST gene in the Saethre-Chotzen syndrome. Nat Genet 1997;15:42–6.

[68] Menashe Y, Ben Baruch G, Rabinovitch O, et al. Exophthalmus–prenatal ultrasonic features for diagnosis of Crouzon syndrome. Prenat Diagn 1989;9:805–8.

[69] Leo MV, Suslak L, Ganesh VL, et al. Crouzon syndrome: prenatal ultrasound diagnosis by binocular diameters. Obstet Gynecol 1991;78:906–8.

[70] Filkins K, Russo JF, Boehmer S, et al. Prenatal ultrasonographic and molecular diagnosis of Apert syndrome. Prenat Diagn 1997;17:1081–4.

[71] Hill LM, Grzybek PC. Sonographic findings with Pfeiffer syndrome. Prenat Diagn 1994;14:47–9.

[72] Bernstein PS, Gross SJ, Cohen DJ, et al. Prenatal diagnosis of type 2 Pfeiffer syndrome. Ultrasound Obstet Gynecol 1996;8:425–8.

[73] Ashby T, Rouse GA, De Lange M. Prenatal sonographic diagnosis of Carpenter syndrome. J Ultrasound Med 1994;13:905–9.

[74] Pandya PP, Kondylios A, Hilbert L, et al. Chromosomal

defects and outcome in 1015 fetuses with increased nuchal translucency. Ultrasound Obstet Gynecol 1995; 5:15–9.

[75] von Kaisenberg CS, Nicolaides KH, Brand-Saberi B. Lymphatic vessel hypoplasia in fetuses with Turner syndrome. Hum Reprod 1999;14:823–6.

[76] Mychaliska GB, Bealer JF, Graf JL, et al. Operating on placental support: the ex utero intrapartum treatment procedure. J Pediatr Surg 1997;32:227–30 [discussion: 230–1].

[77] Marler JJ, Fishman SJ, Upton J, et al. Prenatal diagnosis of vascular anomalies. J Pediatr Surg 2002;37:318–26.

[78] Boon LM, Enjolras O, Mulliken JB. Congenital hemangioma: evidence of accelerated involution. J Pediatr 1996;128:329–35.

[79] Enjolras O, Mulliken JB, Boon LM, et al. Noninvoluting congenital hemangioma: a rare cutaneous vascular anomaly. Plast Reconstr Surg 2001;107:1647–54.

[80] Berenguer B, Mulliken JB, Enjolras O, et al. Rapidly involuting congenital hemangioma: clinical and histopathologic features. Pediatr Dev Pathol 2003 [Epublication; published online 5 Nov 2003].

[81] Schwartz MZ, Silver H, Schulman S. Maintenance of the placental circulation to evaluate and treat an infant with massive head and neck hemangioma. J Pediatr Surg 1993;28:520–2.

[82] Boon LM, Fishman SJ, Lund DP, et al. Congenital fibrosarcoma masquerading as congenital hemangioma: report of two cases. J Pediatr Surg 1995;30:1378–81.

[83] Boulinguez S, Teillac-Hamel D, Bedane C, et al. Cervicofacial hemangioma and a minor sternal malformation: inclusion in PHACES syndrome? Pediatr Dermatol 1998;15:119–21.

[84] Frieden IJ, Reese V, Cohen D. PHACE syndrome. The association of posterior fossa brain malformations, hemangiomas, arterial anomalies, coarctation of the aorta and cardiac defects, and eye abnormalities. Arch Dermatol 1996;132:307–11.

[85] Aeby A, Guerrini R, David P, et al. Facial hemangioma and cerebral corticovascular dysplasia: a syndrome associated with epilepsy. Neurology 2003;60:1030–2.

[86] Grosso S, De Cosmo L, Bonifazi E, et al. Facial hemangioma and malformation of the cortical development: a broadening of the PHACE spectrum or a new entity? Am J Med Genet 2004;124A:192–5.

[87] Pascual-Castroviejo I, Viano J, Moreno F, et al. Hemangiomas of the head, neck, and chest with associated vascular and brain anomalies: a complex neurocutaneous syndrome. AJNR Am J Neuroradiol 1996; 17:461–71.

[88] Bouchard S, Johnson MP, Flake AW, et al. The EXIT procedure: experience and outcome in 31 cases. J Pediatr Surg 2002;37:418–26.

[89] Gripp KW, Stolle CA, Celle L, et al. TWIST gene mutation in a patient with radial aplasia and craniosynostosis: further evidence for heterogeneity of Baller-Gerold syndrome. Am J Med Genet 1999;82: 170–6.

[90] Seto ML, Lee SJ, Sze RW, et al. Another TWIST on Baller-Gerold syndrome. Am J Med Genet 2001;104: 323–30.